Development of Technology for Separation and Enrichment of Nano-Aerosol Particles

ナノ・エアロゾル粒子の高速分級・濃縮技術の開発

（課題番号 15560651）

平成 15 年度～平成 16 年度科学研究費補助金（基盤研究（C）(2)）研究成果報告書

平成 17 年 3 月

研究代表者　古内　正美

（金沢大学大学院自然科学研究科）

目次

はしがき

本研究は平成１５年度～平成１６年度の間に、平成１５年度科学研究費（基盤研究（C）（2））で実施した

「ナノ・エアロゾル粒子の高速分級・濃縮技術の開発」

の成果をまとめたものである。

研究組織

研究代表者：古内　正美（金沢大学大学院自然科学研究科助教授）
研究分担者：畑　光彦（金沢大学大学院自然科学研究科助手）

交付決定額（配分額）（金額単位：千円）

	直接経費	間接経費	合　計
平成 15 年度	2,700	0	2,700
平成 16 年度	1,000	0	1,000
総　計	3,700	0	3,700

研究発表

（１）学会誌等

1) 古内正美，坂野健夫，木津良一，清水良保，大久保敬久，金岡千嘉男，超音速インパクターで分離・捕集された微小大気エアロゾル中の PAHs 成分,エアロゾル研究,印刷中,2005
2) M. Furuuchi, K. Gotoh, C. Kanaoka, The influence of humidity on dry separation of granular particles based on geometrical characteristics, Powder Technology, 2005 in press
3) M. Furuuchi, C.Kanaoka, Y. Shimizu, Separation Characteristics of a Supersonic Virtual Impactor, Proc. Asian Pacific Confederation of Chemical Engineering 2004 (APCChE2004), CD-ROM, 2004
4) M. Furuuchi, C.Kanaoka, Y. Shimizu, High Speed Sampling of Ultra-fine Ambient Particles using Supersonic Flow, Proc. Asian Pacific Confederation of Chemical Engineering 2004 (APCChE2004), CD-ROM, 2004
5) M. Furuuchi and C. Kanaoka, Influence of Geometry of Supersonic Virtual Impactor on Separation Performance of Ultra-fine Aerosol Particles, Proc. 3rd Asian Aerosol Conference, Hong Kong, pp.135a-135b, 2004

（２）口頭発表

1) 古内正美，金岡千嘉男，超音速バーチャルインパクターの微粒子分離特性に及ぼす装置形

状の影響, 日本エアロゾル学会第 20 回エアロゾル科学・技術研究討論会, つくば, 2003 年 7 月

2) 古内正美, 坂野健夫, 清水良保, 金岡千嘉男, 超音速流れを用いた微小大気エアロゾルの高速サンプリング, 日本エアロゾル学会第 20 回エアロゾル科学・技術研究討論会, 札幌, 2004 年 7 月

3) 古内正美, 清水良保, 金岡千嘉男, 超音速バーチャルインパクターの粒子分離特性, 化学工学会第 69 年会, 大阪, 2003 年 3 月

（３） 出版物

直接関連した出版はなし。

研究成果による工業所有権の出願・取得状況

なし

1　背景

気相合成で得られる超微粒子は、液相法に比べて高純度な反面、低圧あるいは不活性雰囲気で生成されるので、数ナノから数ミクロンと極めて広い粒径分布を持ち、一旦集めてしまうとハンドリング性も極めて悪い。このため、その特性を生かすには、浮遊したまま生成粒子を分離・分級することが欠かせない。さらに問題なのは、生成粒子の濃度を高めるのが困難な場合が多いため、生成ナノ粒子を用いた製品の製造効率が著しく低いことである。これらの問題を解決するには、高い処理能力を確保した上で、生成ナノ粒子を浮遊状態のまま任意の濃度に分級・濃縮する技術の確立がどうしても必要である。

気相中での粒子分離・分級法として広く使用されているのは、粒子に作用する慣性力を利用する方法である。この方法では粒子ー流体間相対速度が大きいほど、気流の速度勾配が大きいほど、さらに、運動方向が急激に変化するほど分離径が小さくなり、より小さい粒子の分離･分級が可能となる。しかし、従来の方法が用いる亜音速域の気流速度では、分離・分級できる下限粒子径は 0.3μm 程度と、気相法で合成された超微粒子の分離・分級には全く使えない。したがって、ナノサイズ域で、精度良く粒子を浮遊状態のまま分離・分級できる方法を新たに開発する必要がある。

超音速気流中に障害物を置くと、障害物直前に定在衝撃波が形成される。定在衝撃波を気流が通過する際にはその速度､方向､圧力などが急激に変化するので、このような流れに置かれた粒子には、従来の装置では得られない大きな慣性力が作用し、極微細な粒子でも障害物に衝突・捕集される。さらに、障害物に開孔部を設け、そこから若干の気流を吸引すれば本来障害物に衝突・沈着する粒子を浮遊状態で取り出すことが可能となり、ナノサイズ粒子の分級・濃縮が達成できる。このような「超音速バーチャルインパクター」とも呼ぶべきナノ粒子分級・濃縮技術が確立できれば、ナノ粒子を素材とする先端材料の開発に大きく貢献すると考えられる。

研究目的

本研究では、超音速流れ中に置かれた開孔部を持つ障害物の前方に形成される衝撃波面前後で生ずる粒子運動の急激な変化を利用して、従来形式の分離装置では不可能なナノサイズ粒子の超微粒子の分級・濃縮を高処理量で達成する、超音速バーチャルインパクターを開発することを目標とし、以下の研究を行う。

1）　ラバールノズルで形成された超音速場中に、開孔部を持つ障害物（捕集プローブ）を置き、ノズル内部､障害物近傍､開孔部内の流れを数値シミュレーションにより解析し、高精度のナノ粒子分離を達成する上で重要な、よどみ点流れおよび明瞭な定在衝撃波を形成するために必要なノズル出口周囲の形状、開孔部寸法、幾何学形状、ノズル出口ー捕集プローブ間距離を決定する。

2）　1）で決定されたノズル構造、操作条件に基づき分離・濃縮装置を試作し、その性能を検討する。

1）、2）の結果に基づき、実装置を設計に対する指針を得るとともに、TiO_2光触媒エアロゾルによる有害物質除去の応用技術に検討を加え､本手法の実用性を検証する。

2 ナノエアロゾル粒子分離・濃縮特性に及ぼす装置構造の影響に関する数値解析的検討

2－1 概要

A supersonic dichotomous sampler with a Laval nozzle was numerically investigated into its performance either as a separator or a concentrator for ultra-fine aerosol particles down to nano-size ranges. Influences of the impactor geometry, such as shape of nozzle cross-section (rectangular and circular), clearance between nozzle exit and particle collection probe inlet, and probe geometry on the separation characteristics were simulatively investigated. The effect of sheath flow along the nozzle wall and center on the separation characteristics and the particle wall loss were also analyzed.

The supersonic dichotomous sampler was designed to make the flow as similar to the stagnation flow, which provided a distinct standing shock wave between the nozzle exit and the collection probe inlet. The smaller distance from the collection probe inlet to the standing shock wave was related to the cutoff size of particle. The sheath air flow improved the separation sharpness and reduced the particle wall loss.

2－2 本文

INTRODUCTION

Nanoparticles receiving increasing attention in both technological applications where improved measurement is needed to facilitate process control (Akedo et al., 2003) and environmental science. Increasing concern over the health consequences of ultrafine particles, and especially those in the low nanometer size regime pose serious measurement challenges.

The fine mode of ambient aerosol has been shown to have serious health effects (Spurny, 1999), and has received considerable attention in recent years. However, in order to assess potential health effects of ambient nanoparticles, methods are needed to determine their composition. A number of online measurement methods (TOF-MS; Phares et al., 2001; Suess et al., 1999) and other technologies (e.g., Myojo et al., 2002) have been developed to sample and perform size resolved measurements of the chemical composition of the ambient aerosol. Although the number of constituents of the atmospheric aerosol that can be positively identified by these methods of single-aerosol-particle, the analysis of heavy metals, water solubles, carbon, PAHs, N-PAHs, radionuclides provides information on the emission sources and potential health consequences of atmospheric nanoparticles (Furuuchi and Komura et al., 2002; Tang et al., 2004). Unfortunately, due to the low mass concentrations of these small particles, the

time required to obtain quantitative measurements is frequently so long that the aerosol composition changes significantly during the course of the measurement. One way to overcome this limitation would be to develop a method to concentrate the ultrafine particles while retaining them in an aerosol state.

Methods that would enable concentration of ultrafine particles from large volumes of air would aid in both the development of nanoparticle technology and in understanding atmospheric nanoparticles. Kanaoka et al. (1996, 2001) recently demonstrated that ultrafine particles could be collected by inertial impaction using supersonic jets produced with a Laval nozzle. In this impactor, the aerosol flow is accelerated to supersonic velocities and then impacted to the fixed collection plate. When an obstacle such as a collection plate is placed in the supersonic flow, a standing shock wave upstream of the obstacle. The velocity and direction of motion abruptly change as the gas passes through this so-called "bow shock" and is deflected around the obstacle, causing the particle to experience significant inertial effect s. Early descriptions of particle separation by impaction in underexpanded sonic jets in a low pressure impactor (Hering et al., 1978) noted that the decrease in pressure caused by the flow expansion reduces particle drag and enhances the inertial effect. Later studies revealed that the effect was less pronounced than originally thought, however. Downstream of the shock wave, the gas is recompressed to the upstream stagnation pressure, which can approach the pressure upstream of nozzle entrance (Flagan, 1982, Biswas and Flagan, 1984), so the particles decelerate from supersonic velocities in this high pressure gas flow. de la Mora et al. (1988, 1990, 1998) have shown how these same inertial effects have can be used for hypersonic focusing and impaction of ultrafine aerosol particles. The separation performance depends on the geometry of the impactor such as the shape of Laval nozzle and collection plate size as well as the distance between nozzle exit and the collation plate (Kanaoka et al, 2001).

The dichotomous sampler has been regarded as a continuous size classifier or concentrator of aerosol particles (Chen et al., 1985; Loo et al., 1988; Chen et al., 1994; Masuda et al., 1979, 1984, 1986; Marple et al., 1995, 1995; Pakkanen et al., 1995). Sioutas et al. (1994, 1996, 1997, 1999) have used a dichotomous sampler system as an ambient aerosol concentrator for animal exposure studies to probe health effect of directly sampled ambient particles. Ondov et al. (1996) developed a condensing dichotomous sampler sampling ambient PM to monitor the concentration and chemical components with high time resolution. The present authors have proposed a "supersonic dichotomous sampler" that incorporates supersonic flow into a dichotomous sampler to enable continuous high speed separation of aerosol nanoparticles, and have explored the performance of the device (Kanaoka et al., 2000; Furuuchi et al., 2001, 2002, 2004). Those studies noted that artifacts due to condensation or evaporation of semi-volatiles and water vapor in the supersonic flow could become an important issue in ambient sampling (Furuuchi et al., 2004). Experimental investigations of a supersonic dichotomous sampler with a

different geometry have been reported by Chen et al.(2001) , Poshin et al.(2002) and Pui(2004).

In this study, the supersonic dichotomous sampler with a Laval nozzle was numerically investigated to probe its performance as a separator and a concentrator for ultra-fine aerosol particles down into the nano-size ranges. The influence of the sampler geometry, including the shape of nozzle cross-section (rectangular and circular), the clearance between nozzle exit and collection probe inlet, and the probe geometry, on separation characteristics were explored. The effect of sheath air flow was evaluated in regard to the separation characteristics and the particle wall loss.

NUMERICAL SIMULATION

Geometry of the Supersonic Dichotomous sampler

The supersonic dichotomous sampler consists of a Laval nozzle and a collection probe. The Laval nozzle was used to produce a controlled supersonic flow. By adjusting the length and width, different sizes of nozzles can be designed to produce supersonic flow. **Figure 1** shows the two geometries of supersonic dichotomous samplers studied here: (a) type-A: a wide flat impaction plate, with a collection probe inlet at the center of the plate, that has been designed to obtain a flow similar to that in a plate impactor; (b) type-B: a sharp-edged collection probe to allows rapid expansion of the flow around the collection probe. Both sampler types can be configured with rectangular (slit-type) and circular cross section nozzles. The slit-type nozzle can be easily scaled up to obtain high flow rates. The circular nozzle is expected to provide greater inertial effects due to the rapid expansion of flow downstream the nozzle exit that should lead to a smaller cutoff size. The corners of the collection probe in the type-A sampler are rounded to minimize separation of the boundary layer.

The Laval nozzle was designed to accelerate the flow up to Mach 2 at the nozzle exit, using the following equation (Sabersky et al., 1999; Kanoaka et al., 1996):

$$\frac{A}{A^*} = \frac{1}{M}\left\{\frac{2}{\gamma+1}\left(1+\frac{\gamma-1}{2}M^2\right)\right\}^{\frac{\gamma+1}{2(\gamma-1)}} \qquad (1)$$

where A^*, A and γ are the cross-sectional area of nozzle at the throat, the cross-sectional area

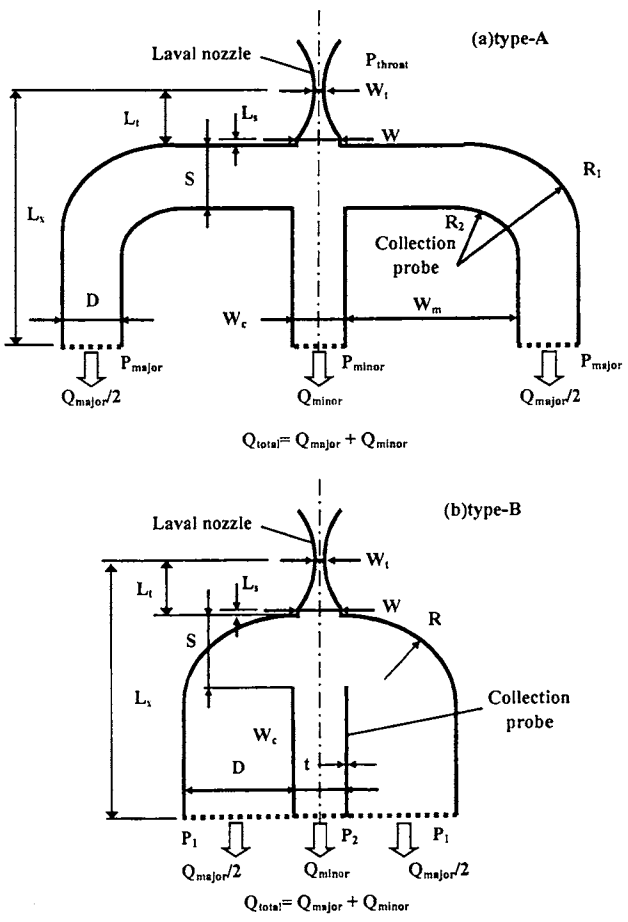

Figure 1. Calculated geometries of supersonic dichotomous sampler.

through which the flow passes with Mach number M, and specific heat ratio, respectively. The shape of the nozzle was designed based upon experimental observations of separation in a slit-type Laval nozzle (Kanaoka et al., 2001).

Sheath Air Flow

Previous studies of low velocity (subsonic) dichotomous samplers (sometimes called a "virtual impactor") does not produce size cuts that are as sharp as (Conner, 1966; Yoshida et al., 1978). Some of the coarse fraction, which ideally would exit the dichotomous sampler through the collection tube, is retained in the major flow or deposits on the wall. At the same time, small particles in the flow near the center of the nozzle that ideally would be excluded from the concentrated sample are carried with the minor flow through the collection probe. Thus, the separation efficiency cannot be reduced below the ratio of the sampling flow rate to collection probe to the total flow rate. The separation efficiency is further reduced, and the cut-off size is increased by eddies. Particle flow near the wall increases the particle wall deposition of particles around the probe inlet (Masuda et al., 1979, 1988). Masuda et al. (1979, 1988) achieved much sharper separations dichotomous sampler by introducing these clean sheath and core air flows into in both circular and rectangular jet designs.

(Masuda et al., 1988).

In the present study, the effectiveness of the addition of sheath flows of the particle-free clean air along the nozzle wall and center as illustrated in Figure 2. The clean sheath air has the thickness of H_1 in the nozzle center side and H_2 in the wall side. In the circular nozzle, an annular aerosol flow surrounded by the clean air was introduced to the nozzle. H_1 and H_2 was adjusted in the rage $<W_t/2$ and corresponding ratio of the sheath flow rate Q_{sheath} to the total flow rate Q_{total} was in the range 0.2-0.8.

Calculation Procedures

Two-dimensional calculations were conducted for the calculation domain shown by hatched areas in Figure 1 using FLUENT ver.6.02, where the fluid was assumed to be viscous and compressible. The k-ε model was used to describe the turbulent dissipation (Shih et al., 1995) . The dimensions of the geometries simulated and boundary conditions are summarized in **Table1**. **Figure 3** shows the mesh network consisting of ca. 40000-60000 cells in all cases. The explicit and segregated computational scheme was employed for the steady state calculation. The calculation was terminated when relative changes in all variables after each calculating iteration become less than 5×10^{-4}. At the inflow and

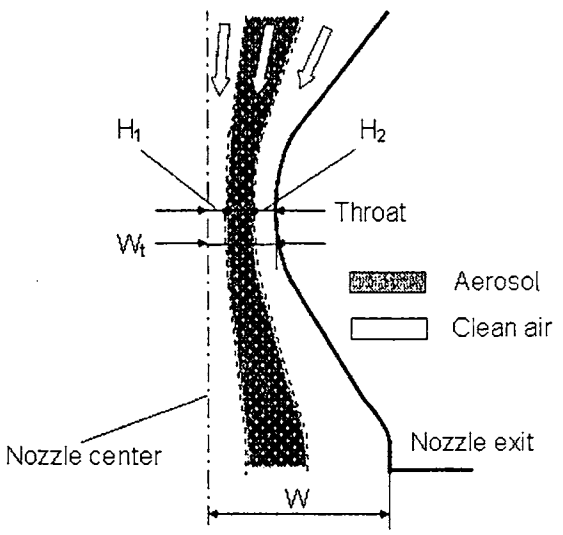

Figure 2. Sheath airflow along the nozzle center and wall where the thickness H_1 and H_2 of clean airflow are defined at the nozzle throat.

outflow boundaries of the calculating area, pressure and k, ε conditions are set. The turbulent length scale is equal to $0.07L$, where L is the reference dimension of either the width of throat, collection probe or major flow outlet.

The flow rate ratio Q_{minor}/Q_{total} was adjusted by changing P_{minor}, the probe outlet pressure: Q_{minor}/Q_{total} increases as decreasing P_{minor}. Since the adjustable range of P_{minor} to obtain the standing shock without a reverse flow from the probe outlet is not so broad even for the same nozzle cross-sectional geometry, the difference in the range of P_{minor} was rather large between the different nozzle cross-sectional geometries.

Particle trajectories were calculated using a user-defined function, in which Cunningham correction factor C_c was expressed as a function of pressure and temperature inside the calculation element including a particle by the equation by Allen et al (1982) as follows:

$$C_c = 1 + \frac{\lambda}{d_p}\left\{2.34 + 1.05\exp\left(-0.39 d_p / \lambda\right)\right\} \quad (-) \qquad (2)$$

where d_p is the particle diameter and λ is the mean free path of air molecule determined from the following equation (Willeke, 1976):

$$\lambda = 0.0665 \cdot \frac{101300}{P} \cdot \frac{T}{293.15} \cdot \frac{1+110.4/293.15}{1+110.4/T} \quad (\mu m) \qquad (3)$$

where P is the static pressure and T is the temperature. And the drag coefficient for spherical particles expressed by the following equation was used (Haider et al, 1989):

$$C_D = \frac{24}{\mathrm{Re}_p}\left(1 + 0.1806\,\mathrm{Re}_p\right) + \frac{0.4251}{1 + 6880.95/\mathrm{Re}_p}$$

$$\mathrm{Re}_p = \frac{\rho|u - v|d_p}{\mu} \qquad (4)$$

where Re_p is the particle Reynolds number, u is fluid velocity, v is particle velocity and μ is fluid viscosity.

As particles pass through a shock wave, they are injected into a subsonic flow at

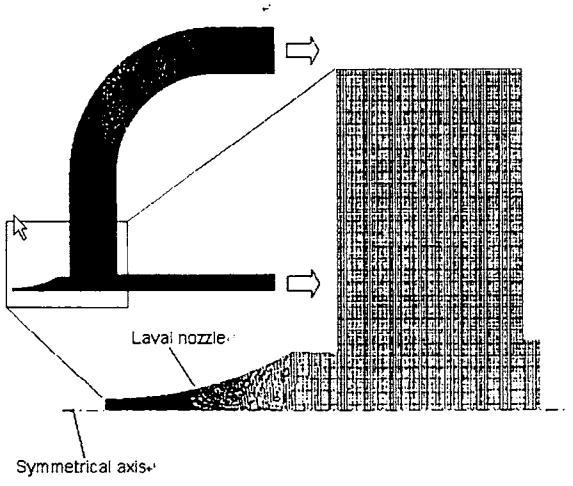

Figure 3. Mesh network for calculation

Table 1 Dimensions of supersonic dichotomous samplers and boundary conditio

Nozzle geometry	type-A	type-B
W_t (mm)	1	
L_t (mm)	10	
L_s (mm)	2	
L_c (mm)	45	
R (mm)	-	15
R_t (mm)	15	-
R_c (mm)	R_t+D	-
S (mm)	5,8,11,14	11
W (mm)	5	
W_{in} (mm)	6,8,9	6
W_{out} (mm)	32	-
D (mm)	5,8,11,14	14
Static pressure at nozzle throat P_{throat}	53.5kPa	
Static pressure of major flow exit P_{major}	0.1kPa	
Static pressure of minor flow exit P_{minor}	3.2~22kPa	3.2~32kPa
Turbulence intensity at inlet and outlet (%)	5%	
Turbulent flow length	0.07L (L:corresponding boundary scale)	
Initial particle velocity (m/s)	Sonic velocoty at nozzle throat	

supersonic velocities, so the compressible flow effects need to be taken into account, i.e., $C_D = C_D(Re_p, M_p)$, where M_p is the particle Mach number defined by $|u-v|/a$ where a is the local sound velocity. (Henderson, 1976; Flagan, 1982; Biswas et al, 1988; Oskouie et al., 1998, 2002). Henderson (1976) proposed to use the following equations for the drag coefficient as a function of Re_p and M_p:

$M_p \le 1$

$$C_D = 24\left[\mathrm{Re}_p + R\left\{4.33 + \left(\frac{3.65 - 1.53T_p/T_g}{1 + 0.353T_p/T_g}\right)\right\}\exp\left(-0.247\frac{\mathrm{Re}_p}{R}\right)\right]^{-1} + \exp\left(-\frac{0.5M_p}{\sqrt{\mathrm{Re}_p}}\right)\left[\frac{4.5 + 0.38(0.03\mathrm{Re}_p + 0.48\sqrt{\mathrm{Re}_p})}{1 + 0.03\mathrm{Re}_p + 0.48\sqrt{\mathrm{Re}_p}} + 0.1M_p^2 + 0.2M_p^8\right] + \left[1 - \exp\left(-\frac{M_p}{\mathrm{Re}_p}\right)\right]\cdot 0.6R \quad (5)$$

$1.75 > M_p > 1$

$$C_D = C_D(1.0, \mathrm{Re}_p) + \frac{4}{3}(M_p - 1.0)\left[C_D(1.75, \mathrm{Re}_p) - C_D(1.0, \mathrm{Re}_p)\right] \quad (6)$$

$M_p \ge 1.75$

$$C_D = \frac{0.9 + \frac{0.34}{M_p^2} + 1.86\left(\frac{M_p}{\mathrm{Re}_p}\right)^{1/2}\left[2 + \frac{2}{R^2} + \frac{1.058}{R}\left(\frac{T_p}{T_g}\right)^{1/2} - \frac{1}{R^4}\right]}{1 + 1.86\left(\frac{M_p}{\mathrm{Re}_p}\right)^{1/2}} \quad (7)$$

where R is the molecular speed ratio equal to $M_p\sqrt{\gamma/2}$, T_p is the temperature of particle, which is assumed to be isothermal, and T_g is the gas temperature. The particle trajectory was calculated in the flow field, neglecting both the influence of particle motion on the flow field and the Brownian motion. Particles having sonic velocity along the nozzle axis were released at the nozzle throat. Results evaluated using Eqs.(2) and (4) for the particle drag were compared with those using Eqs.(5)-(7). Variables of the flow field, such as pressure, temperature and velocity, used to calculate the particle motion were those in each element where a particle locates.

RESULTS AND DISCUSSION

Influence of Sampler Geometry on Flow Field

Figures 4 and **5** show the local Mach number distribution inside the type-*A* sampler for rectangular and circular nozzles with a clearance to nozzle width ratio of S/W=1.6, respectively. The profile of static pressure P normalized by the ambient pressure P_0 is also plotted in these figures. The flow accelerates to the supersonic velocity at the nozzle exit, and then continues to accelerate as it expands into the low pressure region. The flow velocity then abruptly decreases in front of the collection probe inlet where the standing shock wave leads to a discontinuous increase in the static pressure. The distance of the standing shock from the collection probe inlet is reduced by the continued expansion of the jet downstream of the nozzle exit. Since the larger expansion is obtained for the circular nozzle, the flow produces a higher axial velocity rapidly and a standing shock wave closer to the probe inlet than the rectangular nozzle. As the deflected flow expands radially outward, it again accelerates to supersonic velocity, as observed by Flagan (1982) in simulations of low pressure impactors operated with sonic jets. The rectangular nozzle sampler shown in Figure 4 has the flow rate ca. $10T$ m^3/min, where T is the nozzle depth in meters while the circular nozzle sampler (Figure 5) has ca. 8×10^{-3}m^3/min. Since

there may be no technological difficulty to increase T up to 0.1-0.2 m, the rectangular nozzle has a large advantage in the flow capacity to realize the sampling rate of 1-2m^3/min., provide adequate pumping capacity is available.

Figure 6(a), (b) and (c) respectively shows the local Mach number distribution for a collection probe width W_c/W of 1.3, 1.6 and 1.8 mm at S/W =2.2. The geometry and position of the standing shock wave are affected by the nozzle width. When W_c/W is less than 1.6, flat standing shock wave is formed; however, for W_c/W=1.8, the standing shock wave almost disappears. This may refer to that there is a critical W_c/W for the shock formation, above which the flow around the collection probe inlet is similar to the flow impacting flat plate. In the following calculations, W_c/W = 1.2 was used to obtain the standing shock. The critical W_c/W value may be affected by the nozzle geometry and flow condition and will be discussed in the future work.

For different clearance-nozzle width ratios S/W, Figure 7(a) and (b) show the Mach number along the celnterline, M_0, for Q_{minor}/Q_{total} = 0.12 and 0.23, respectively, where Q_{total} is the total flow rate and Q_{minor} is the flow rate through the collection probe. In the calculations, the ratio Q_{minor}/Q_{total} was adjusted by changing P_{minor} to obtain a given value. The position of the standing shock wave moves closer to the nozzle exit as S/W decreases. A big difference in the position of the standing shock wave due to the collecting flow rate ratio could be seen at S/W=1. At Q_{minor}/Q_{total} = 0.12, the standing shock wave locates almost at the nozzle exit, disturbing the flow inside the nozzle.

The sharp-edged collection probe has

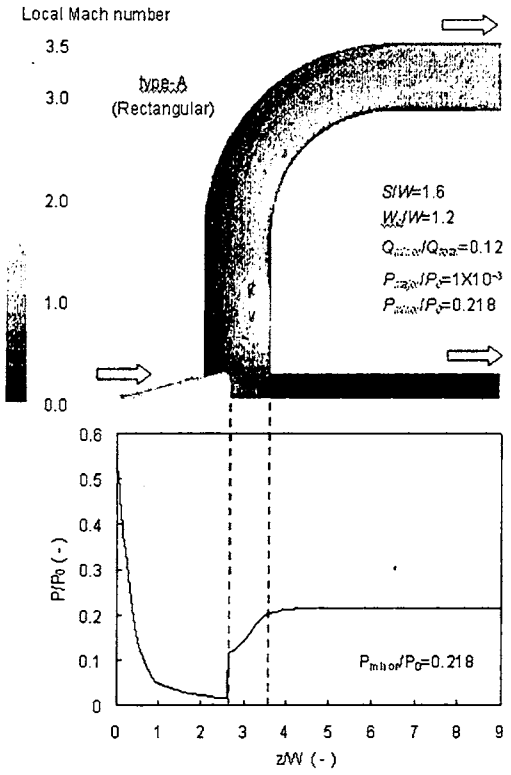

Figure 4. Distribution of fluid local Mach number and the reduced static pressure P/P_0 along the nozzle center (type-*A*, rectangular nozzle), where P_0 is the ambient pressure and z/W is the distance z from the nozzle throat normalized by nozzle width W.

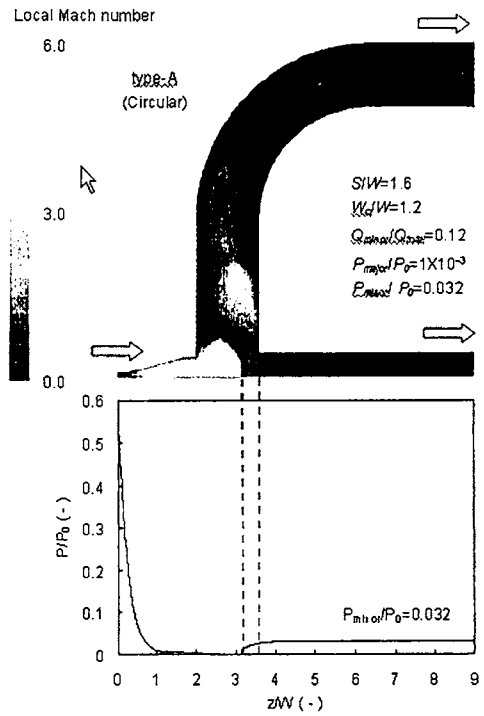

Figure 5. Distribution of fluid local Mach number and the reduced static pressure P/P_0 along the nozzle center (type-*A*, circular nozzle), where P_0 is the ambient pressure and z/W is the distance z from the nozzle throat normalized by nozzle width W.

some possibility to provide a rapid expansion of flow. With Figure 8(a) and (b) showing the local Mach number profiles in the type-*B* nozzles with rectangular and circular nozzles, respectively, the position of the standing shock wave inside the circular nozzle sampler is similar to the type-*A* sampler. The geometry of the standing shock wave is clear cut and the flow after the collection probe is sufficiently decelerated. Contrarily, the standing shock wave inside the rectangular nozzle is distorted, resulting in disappearance of similarity to the stagnation flow.

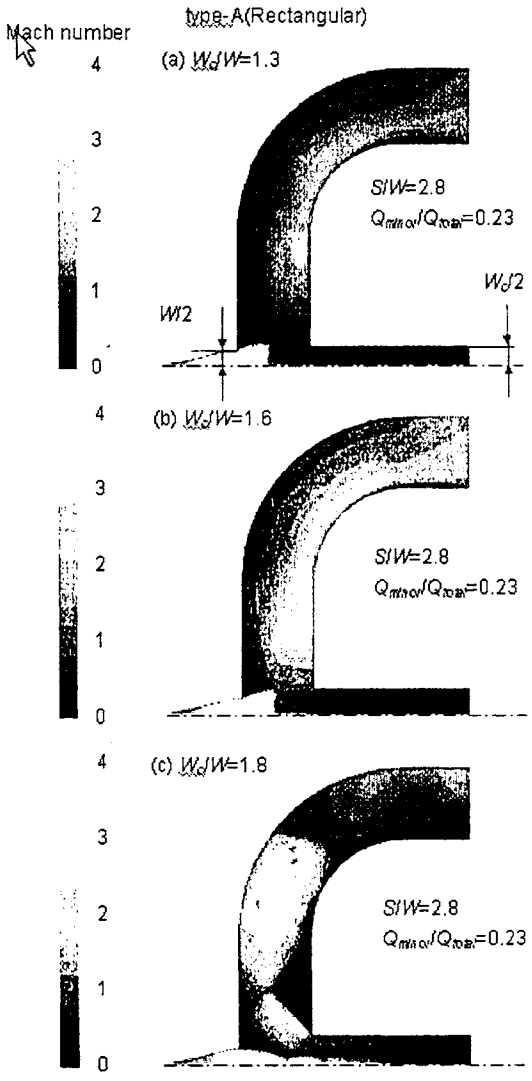

Figure 6. Influence of the collection probe width W_c/W on the formation of standing shock wave.

Figure 9 shows the axial velocity distribution inside the Laval nozzle normalized by the axial velocity at the nozzle center U_0 and the nozzle width Y_{max} at the distance z from the nozzle throat normalized by the nozzle width W. The normalized velocity decreases near the wall similarly at each distance z/W, indicating the boundary layer development, which leads to the lower inertial effect and the particle wall loss. Although the influence of the boundary layer may differ for different designs of nozzle, the importance of the boundary layer development should be noticed. This problem could be solved by supplying some clean air flow along the nozzle wall as shown in later.

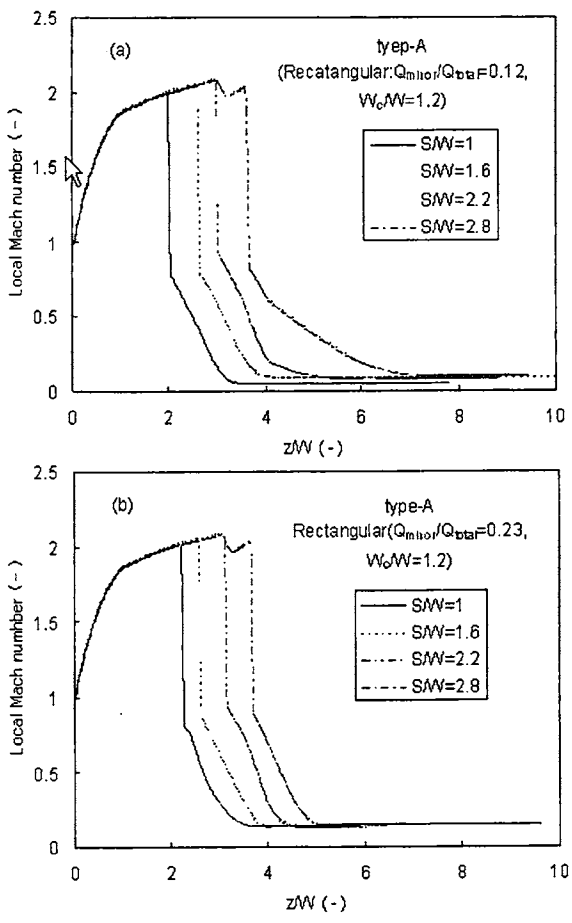

Figure 7. The Local Mach number distribution along the nozzle center in relation S/W.

Particle Trajectory and Separation Characteristics

Figure 10 illustrates particle trajectories inside the sampler for different inertial parameter $\varphi^{1/2}$ (S/W=1.6) defined as Eq.(8) (Biswas et al., 1984):

$$\varphi = \frac{\rho_p U d_p^{\,2}}{18\mu W} C_c \qquad (8)$$

where U is the velocity along nozzle axis at the nozzle exit, fluid viscosity μ and mean free path λ were calculated for the condition at the collection probe exit taking into account the measurable stagnant condition (Flagan, 1982). As the value of inertial parameter increases, particles are concentrated along the nozzle center and, even more, on the collection probe.

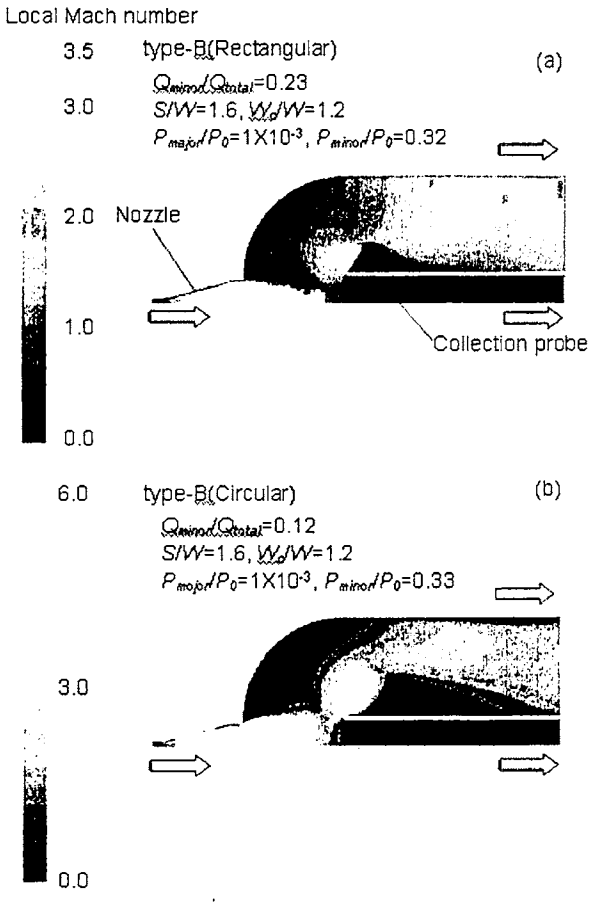

Figure 8. Local Mach number distribution in the type-*B* impactors with different cross sections.

Particles impacting the wall are regarded as "deposited". Figure 11 shows the fractional collection efficiency $\Delta\eta$ of particles for the rectangular nozzle with S/W as a parameter. Particles flowing through the collection probe are defined as "collected" while ones impacting the inner wall of the collection probe are defined as "deposited". The

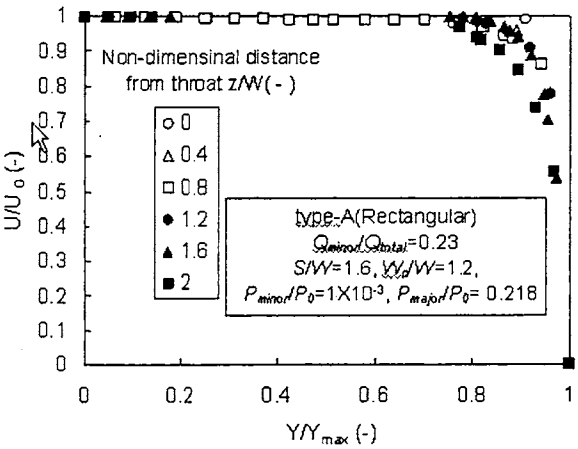

Figure 9. The fluid velocity U along the nozzle axis normalized by U_0 at the nozzle center in relation to the position Y in the nozzle cross section normalized by distance Y_{max} from nozzle center to nozzle wall.

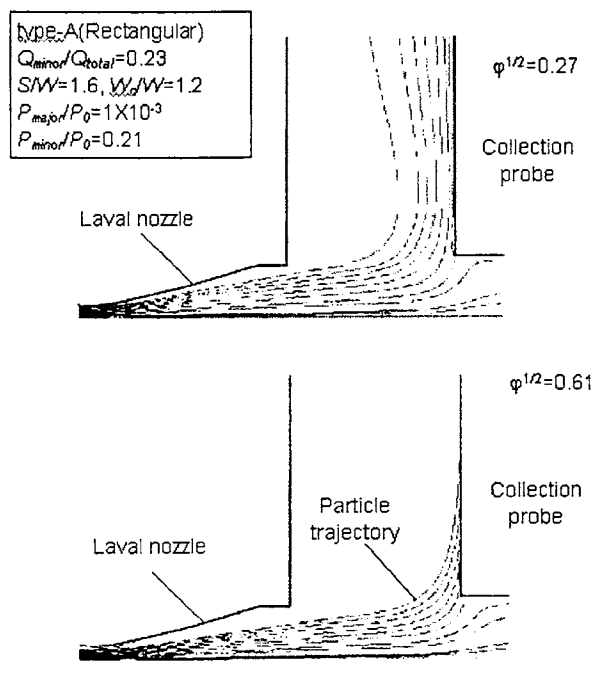

Figure 10. Trajectories of particles with different inertial parameter.

collection efficiency of each size of particle was evaluated from the initial position at the nozzle throat giving the limiting trajectory. The cut-off inertial parameter is almost independent of S/W excepting S/W=1 but the efficiency curve becomes steeper for smaller S/W. Similar but slightly scattered results with S/W were obtained for μ and λ at the ambient condition, which can be also the representative of the stagnant condition (Flagan, 1982). Further decrease in S/W may lead to an increase in disturbance of flow inside the nozzle by the standing shock wave. As shown in Figure 12 for smaller Q_{minor}/Q_{total}, the trend with S/W is same to the larger collecting flow rate. As shown in Figure 13, the collection efficiency curve for the circular is rather complicated. A jump appearing around $\varphi^{1/2} \sim 0.5$ is caused by the deposition of particles with corresponding size are collected on the inner wall of the collection probe. Such deposition can be suppressed by the sheath flow as also shown in Figure 13. The cut-off $\varphi^{1/2}$ value for non-sheath air condition is around 0.5, slightly smaller than the rectangular nozzle, giving a smaller cut off size.

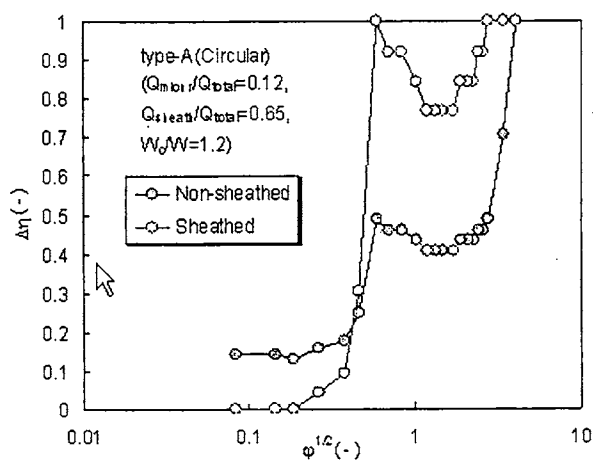

Figure 13. Fractional separation efficiency $\Delta\eta$ of particles in relation to the inertial parameter $\varphi^{1/2}$ and influence of sheath flow (type-*A*, circular, W_c/W=1.2, Q_{minor}/Q_{total}=0.12, Q_{sheath}/Q_{total}=0.65).

Influence of compressibility is discussed in Figure 14, where collection efficiency curves for different nozzle cross-sections are compared between those using Eqs.(2) and (4) and ones using Henderson's equations. The difference is very small for the rectangular nozzle while for the circular nozzle, higher collection efficiencies of particles were evaluated in the range of inertial parameter $\varphi^{1/2} = 1 \sim 4$ using Henderson's equations. This can be related to the fact that the particle Mach number keeps around or exceeds unity even when a particle is passing through the collection probe. This is because of the higher inertial effect in the upstream of the shock and the lower pressure downstream the standing shock. Contrarily, in the rectangular nozzle, the particle Mach number exceeds unity only when a particle passing through the standing shock.

Figure 15 shows the relation between the cutoff inertial parameter $\varphi^{1/2}(50\%)$ size and the distance z_s along the nozzle center between the collection probe inlet and the standing shock wave normalized by the nozzle width W. Data from different nozzle cross-sections, the flow rate ratio Q_{minmor}/Q_{total} are compared taking into account the influence of compressibility. Although the difference $\varphi^{1/2}(50\%)$ is small and the circular nozzle does not have a unique value, there is a trend of a slight increase with z_s/W. This may be due to the larger inertial effect when the standing shock wave approaches to the probe inlet. It

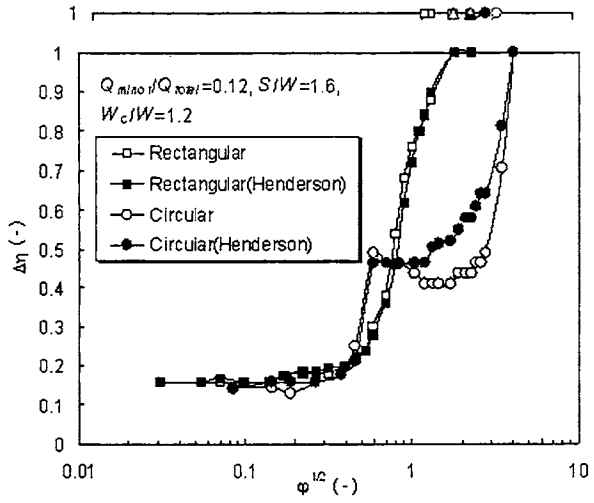

relation to the inertial parameter $\varphi^{1/2}$ for different clearance to nozzle width ratio S/W (type-*A*, rectangular, W_c/W=1.2, Q_{minor}/Q_{total}=0.23).

Figure 14. Influence of fluid compressibility on fractional collection efficiency $\Delta\eta$ of particles (type-*A*, S/W=1.6, W_c/W=1.2, Q_{minor}/Q_{total}=0.12).

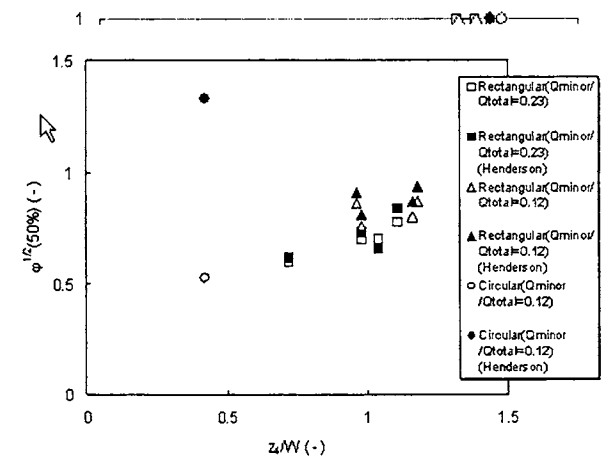

Figure 15. Cutoff inertial parameter $\varphi^{1/2}(50\%)$ plotted against nondimensional distance (z_s/W between the collection probe inlet and the standing shock defined at the nozzle center.

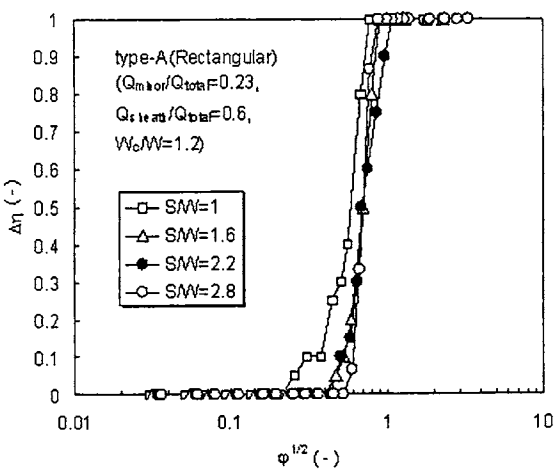

Figure 16. Fractional separation efficiency $\Delta\eta$ of particles in relation to the inertial parameter $\varphi^{1/2}$ for different clearance to nozzle width ratio S/W (type-*A*, rectangular, W_c/W=1.2, Q_{minor}/Q_{total}=0.23, Q_{sheath}/Q_{total}=0.6).

may be important to design so as to efficiently expand the flow after the nozzle. The difference due to the compressibility is clear as seen the collection efficiency curve in Figure 13.

Effect of Sheath Air Flow on Separation Performance and Particle Wall Loss

In Figure 16, the collection efficiency curve in the case of particle free clean air supplied along the wall and center of nozzle is shown. As can be seen by comparing Figures 11 and 16, the sharpness of separation curve increases by supplying the sheath flow while remaining the cut-off inertial parameter almost un-changed. The influence of sheath flow rate ratio Q_{sheath}/Q_{total} is shown in Figure 17, where the total flow rate Q_{total} is kept constant and the sheath flow thickness defined as Figure 2 is set as H_1=H_2. Lager Q_{sheath}/Q_{total} leads to the sharp separation while the flow rate of aerosol, which is important to obtain the larger capacity of separation, decreases. For the circular nozzle, although $H_1 \neq H_2$ for different Q_{sheath}/Q_{total}, the increase in Q_{sheath}/Q_{total} improves the sharpness of separation as similar to the rectangular nozzle.

Figure 18 shows the wall loss of particles inside the rectangular nozzle sampler plotted against the inertial parameter for different clearance ratio *S/W*, where only the wall loss due to inertial impaction was accounted. The wall loss increases around the cutoff inertial parameter and the clearance seems to have only some small influence on the particle deposition. As shown in Figure 19, the particle wall loss decreases especially around the cutoff inertial parameter when the sheath flow is used. The type-*B* sampler with a rectangular nozzle shows some higher portion of particle wall loss because the flow pattern is far from that of the stagnation flow as shown in Figure 8. Figure 20 shows the wall loss inside the circular nozzle sampler. Coarse particles with larger impaction parameter are apt to hit and deposit on the inner wall of collection probe. This is the reason why the decrease in the collection efficiency curve for the circular nozzle is observed. The sheath flow along the nozzle-centerline can reduce such fraction.

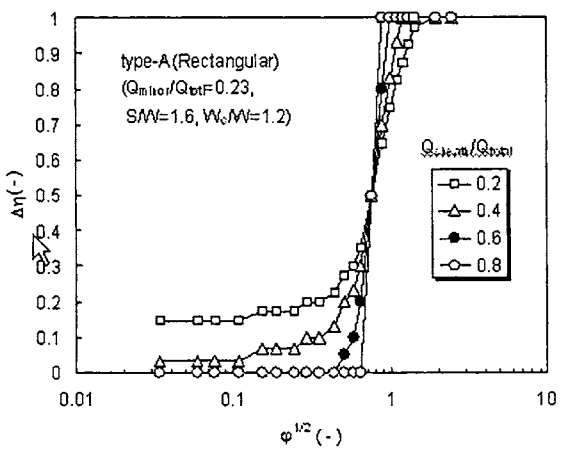

Figure 17. Influence of sheath flow rate ratio Q_{sheath}/Q_{total} on the fractional separation efficiency $\Delta\eta$ of particles (type-*A*, rectangular, W_e/W=1.2, Q_{minor}/Q_{total}=0.23, sheathed).

CONCLUSIONS

Flow and particle motion in the supersonic dichotomous sampler was simulatively investigated in terms of influences of nozzle geometry and operational conditions. Following conclusions could be drawn from achieved results:

1) The standing shock wave can be formed in front of collection probe inlet by adjusting out flow pressures of the supersonic dichotomous sampler.
2) Under the limited condition that the standing shock is formed without any reverse flow from the collection probe outlet, a rapid expansion of flow was found to be effective to reach some higher inertial effect. The smaller cut-off inertial parameter and the higher separation sharpness may be obtained as the position of the standing shock wave moves closer to the collection probe inlet.
3) The fluid compressibility affects the separation performance when a particle keeps the Mach number greater than unity after passing through the standing shock.
4) The separation performance is improved by supplying a sheath air flow along the nozzle wall and center line. The particle wall loss decreased when the sheath flow was used.
5) The nozzle geometry, which provides the flow similar to the stagnation flow at the collection probe inlet, is important for achievement of a better separation performance and less particle deposition.

ACKNOWLEDGEMENT

The authors would gratefully acknowledge valuable comments from editor and reviewers for and would also acknowledge much of help for calculations from Ms T. Sakano.

REFERENCES

Akedo, J. (2003). Review of aerosol deposition method and it's application to MEMS- novel ceramics coating with collision of fine powder at room temperature, *Proc. Int. Conf. Characterization and Control of Interfaces for High Quality Advanced Materials*, Kurashiki, pp.51.

Allen, M. D. and Raabe, O. G. (1982). Re-evaluation of Millikan's oil drop data for the motion of small particles in air, *J. Aerosol Sci.*, 6, 537-547.

Biswas, P. and Flagan, R. C. (1984). High-velocity inertial impactor, *Environ. Sci. Technol.*, 18, 611-616.

Biswas, P. and Flagan, R. C. (1988). The particle trap impactor, *J. Aerosol Sci.*, 19(1), 113-121.

Chen, B. T., Yeh, H. C. and Cheng, Y. S.(1985). A novel virtual impactor: calibration and use, *J. Aerosol Sci.*, 16, 343-354.

Chen, H., Lundgren, D. A. (1994). A virtual

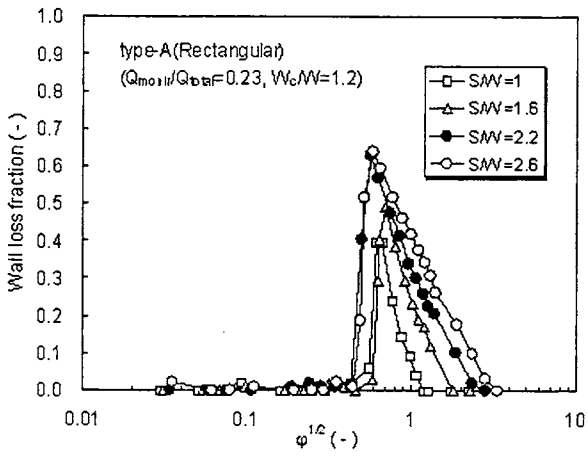

Figure 18. Wall loss of particles in relation to inertial parameter $\varphi^{1/2}$ with the clearance to nozzle width ratio S/W as a parameter (type-*A*, rectangular, W_c/W=1.2, Q_{minor}/Q_{total}=0.23).

Lews Pub., New York (1999)

2) Phares, D. J., Rhoads, K. P., Wexler, A. S., Kane, D. B. and Johnston, M. V.: Application of the ART-2a Algorithm to Laser Ablation Aerosol Mass Spectrometry of Particle Standards, *Anal. Chem.*, **73**, 2338-2344 (2001)

3) Myojo, T., Takaya, M. and Ono-Ogasawara, M.: DMA as a Gas Converter from Aerosol to "Argonsol" for Real-Time Chemical Analysis Using ICP-MS, *Aerosol Sci. Technol.*, **36**, 76-83 (2002)

4) Furuuchi, M., Komura, K., Kizu, R., Kato, S., Limpasami, W., Amornkitbamurung, M. and Kanaoka, C.: New approach to estimate PM emission sources in Bangkok, *Proc. 6th Int. Aerosol Conf.*, Taipei (Edited by Chiu-Sen Wang), 1153-1154 (2002)

5) Hayakawa, K., Tang, N., Akutsu, K., Murahashi, T., Kakimoto, H., Kizu, R. and Toriba, A.: Comparison of Polycyclic Aromatic Hydrocarbons and Nitropolycyclic Aromatic Hydrocarbons in Airborne Particulates Collected in Downtown and Suburban Kanazawa, Japan, *Atmos. Environ.*, **36**, 5535-5541 (2002)

6) Furuuchi, M. and Kanaoka, C.: Numerical Simulation of Flow and Particle Motion inside a Supersonic Virtual Impactor, *Proc. Int. Symp. on Nano-particles,* Pusan, 98-102 (2001)

7) Furuuchi, M. and Kanaoka, C.: Numerical Investigation on Supersonic Virtual Impactor for Separation and Enrichment of Nano-particles, *Proc. 6th Int. Aerosol Conf.*, Taipei (Edited by Chiu-Sen Wang), 1019-1020 (2002)

8) Furuuchi, M. and Kanaoka, C.: Influence of Geometry of Supersonic Virtual Impactor on Separation Performance of Ultra-fine Aerosol Particles, *Proc. 3rd Asian Aerosol Conference,* Hong Kong, 135a-135b (2004)

9) Hill, Ph. G.: Condensation of Water Vapor during Supersonic Expansion in Nozzles, *J. Fluid Mech.*, **25**, 593-620 (1966)

10) Kanaoka, C. and Furuuchi, M.: Inertial Separation of Nano-size Particles from Supersonic Flow Field, *J. Aerosol Sci.*, **29**, S1041-1042 (1996)

11) Kanaoka, C., Uji, N., Furuuchi, M. and Chatomanop, J.: Theoretical Study of Inertial Separation of

Ultra-fine Particles by a Supersonic Impactor, *Proc. First Asian Particle Technology Symp.*, Bangkok, S-VI-7 (2000)

12) Kanaoka, C., Chutmanop, J. and Kitada, M.: Inertial Separation of Ultrafine Particles by a Laval Nozzle Type Supersonic Impactor, *Powder Technol.*, **118**, 188 (2001)

13) Sabersky, R. H., Acosta, A. J., Hauptmann, E. G. and Gates, E. H.: "Fluid Flow", 4th ed., Prentice Hall Int., New Jersey (1999)

14) Shih, T. H., Liou, W.W., Shabbir, A. and Zhu, J.: A New k-ε Eddy-viscosity Model for High Reynolds Number Turbulent Flows – Model Development and Validation, *Computers Fluids*, **24**, 227 (1995)

15) Allen, M. D. and Raabe, O. G.: Re-evaluation of Millikan's Oil Drop Data for the Motion of Small Particles in Air, *J. Aerosol Sci.*, **6**, 537-547 (1982)

16) Willeke, K.: Temperature Dependence of Particle Slip in a Gaseous Medium, *J. Aerosol Sci.*, **7**, 381-387 (1976)

17) Haider, A. and Levenspiel, O.: Drag Coefficient and Terminal Velocity of Spherical and Nonspherical Particles, *Powder Technol.*, **58**, 63-70 (1989)

18) Prast, B., van Dam, A., Willems, J. F. H. and van Dongen, M. E. H.: Formation of Nano-sized Water Droplets in a Supersonic Expansion Flow, *J. Aerosol Sci.*, **27**, S147-S148 (1996)

19) Yamasaki, H., Kuwata, K. and Miyamoto, H.: Effects of Ambient Temperature on Aspects of Airborne Polycyclic Aromatic Hydrocarbons, *Environ. Sci. Technol.*, **16**, 189-194 (1982)

20) Tang, N., Taga, R., Hattori, T., Tamura, K., Toriba, A., Kizu, R. and Hayakawa, K.: Atmospheric Nitorbenzanthrones by Liquid Chromatography with Chemiluminescense Detection, *Anal. Sci.*, **20**, 119-123 (2004)

21) Kameda, Y., Shirai, J. Masunaga, S. Komai, T. and Nakanishi, J.: Size Distributions of Atmospheric PAHs and Dioxin-like Toxicity and Estimation of their Depositions to Human Respiratory Tract, *Proc. 12th Japan Society for Environ. Chem. Symp.*, Niigata (2003)

22) Seinfeld, J and Pandis, S: "Atmospheric Chemistry and Physics", p.743, J. Wiley&Sons, New York (1998)

超音速流れと光触媒エアロゾル粒子を利用した大気中有害ガス成分の高速分解に関する基礎的検討

－光触媒ナノエアロゾル粒子(TiO_2)の気相合成特性の評価－

1 はじめに

超音速流れ場中では極めて高い過飽和状態が作り出されるため、極微量のガス成分であっても固体粒子表面に強制的に凝縮・吸着される。したがって、これを積極的に利用できれば、高い過飽和状態を利用した環境浄化技術にも応用できる可能性も持っている。すなわち、ラバールノズル上流で気相合成した光触媒ナノエアロゾル粒子(TiO_2)を VOC やホルムアルデヒドなどの有害物質で汚染された室内空気と混合し、超音速流れ場中の非常に高い過飽和状態を利用して有害汚染物質を粒子表面に強制的に濃縮し、紫外線照射で生成した OH ラジカルと効果的に反応させれば、除去・分解効率を格段に向上させることが可能となると考えられる。これはすでに立証されているナノ TiO_2 エアロゾルを用いた石炭燃焼排ガス中からの元素水銀蒸気の除去の効率化や、大気中にガス状で存在する多環芳香族炭化水素（PAHs）などの発がん性の物質の除去にも応用の可能性を持っている。

このようなナノ粒子分級・濃縮技術をベースにしたナノ複合材料製造技術、環境浄化技術が確立できれば、ナノ粒子を素材とする先端材料の開発、医療分野、環境浄化に大きく貢献すると考えられる。

本研究では、研究実施期間内にナノ TiO_2 エアロゾルを用いた大気中のガス状・粒子状 PAHs の分解特性の検討に着手し、現在も継続中であるが、ここでは研究期間内に製作したナノ TiO_2 エアロゾルの発生装置の基本特性について検討した結果を報告する。

2 ナノ TiO_2 エアロゾル粒子の発生

ナノ TiO_2 エアロゾル粒子の発生装置の全景を **Fig.1** に、発生フローチャートを **Fig.2** に示す。発生装置はチタニウムテトライソプロポキシド（TTIP）発生部、TiO_2 気相合成部および TiO_2 気相合成特性評価部で構成されている。TTIP は常温では薄黄色透明な液体であり、融点 17℃、沸点 232℃である。TTIP の変質を防ぐためにアルゴン（Ar）ガスをキャリアガスとしている。マスフローコントローラーにより流量制御された Ar ガスを、TTIP が

入ったガス洗浄瓶（恒温水槽で温度コントロール）に供給してバブリングさせることで TTIP 蒸気を発生させ（**Fig.3**）、これに流量制御した清浄乾燥空気を混合し、TiO_2 気相合成部に導入する。TiO_2 気相合成部で TTIP 蒸気は(1)式に従い反応し、TiO_2 ナノエアロゾルを得る。

$$\mathbf{Ti[OCH(CH_3)_2]_4}\ (\mathrm{TTIP}) \rightarrow \mathbf{TiO_2} + 4C_3H_6 + 2H_2O \quad (1)$$

TiO_2 気相合成特性の評価として、発生した TiO_2 エアロゾル粒子を HEPA フィルタで捕集し、その捕集量から発生濃度を、捕集粒子の SEM 観察結果より粒径及び形状を調べた。

TTIP 発生温度 T_1、管状炉内温度 T_2 を変化させ、異なる 5 条件で TiO_2 ナノエアロゾル粒子の発生を試みた。実験

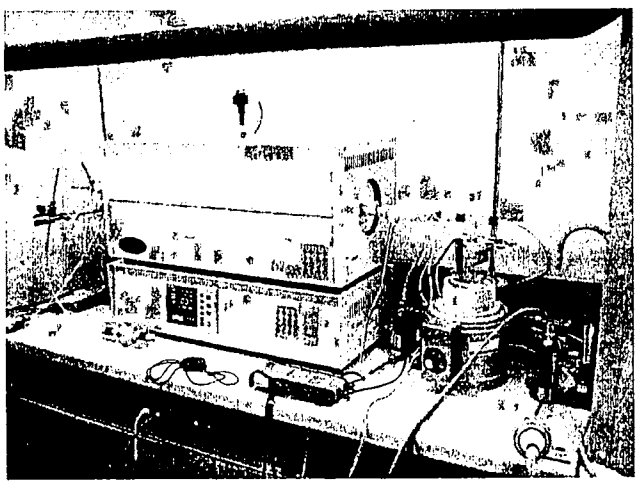

Fig.1 Photograph of experimental setup

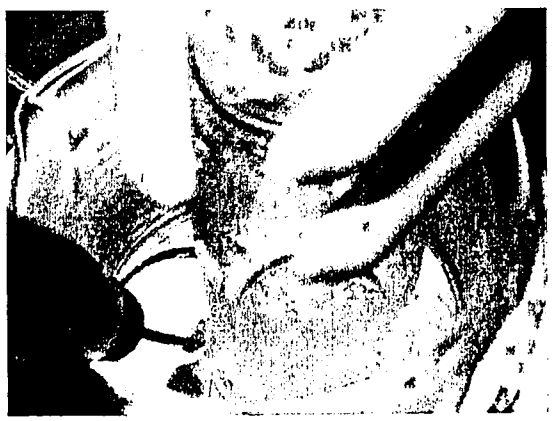

Fig.3 Photograph of TTIP generating

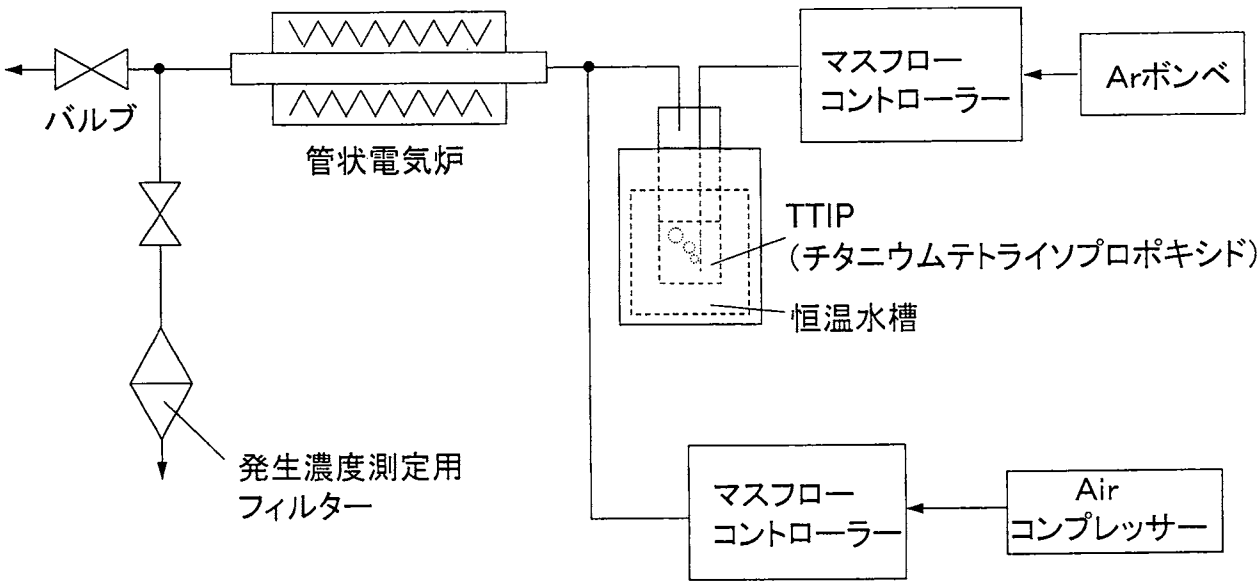

Fig.2 Experimental setup for TiO_2 nano particles generating

条件を **Table 1** にまとめた。

2　発生させた TiO_2 ナノ粒子の評価

Fig.4 に TTIP 発生温度 T_1=70℃、管状炉内温度 T_2=1000℃で発生した TiO_2 粒子濃度を発生時間に対して示した。図より、時間の経過と共に TiO_2 粒子濃度が減少していることより、本発生条件では TiO_2 粒子を長時間安定した濃度で発生させられないことがわかる。そこで、T_1=75℃、T_2=1050℃で TiO_2 粒子を発生させることを試みた。発生濃度の経時変化を **Fig.5** に示す。図より、発生開始から 100 分程度は濃度が減少しているが、その後はほぼ一定の発生濃度を保っていることから、本発生条件を有害汚染物質の連続的に除去・分解するための発生条件として採用することとした。

Fig.6 は、Fig.5 と同様の発生条件で発生より 210 分経過した際に HEPA フィルタ上に TiO_2 粒子を捕集した SEM 写真の一例である。捕集時間が 30 分であるため TiO_2 粒子同士が凝集しているが、一次粒子径は数十 nm である。よって、本方法で気相合成した TiO_2 ナノエアロゾル粒子をラバールノズル上流で①VOC やホルムアルデヒドなどの有害物質で汚染された室内空気、②大気中の半揮発性成分である多環芳香族炭化水素類（PAHs）と混合し超音速流れ場中に導入することで、これらの有害汚染物質を非常に高い過飽和度により TiO_2 ナノ粒子表面に強制的に

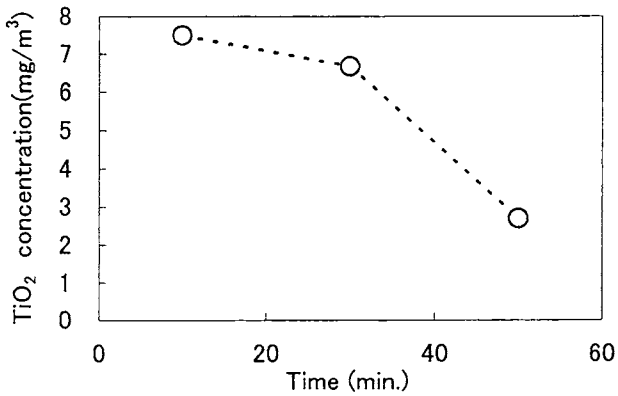

Fig.4 Change of TiO_2 concentration with time (T_1=70℃, T_2=1000℃)

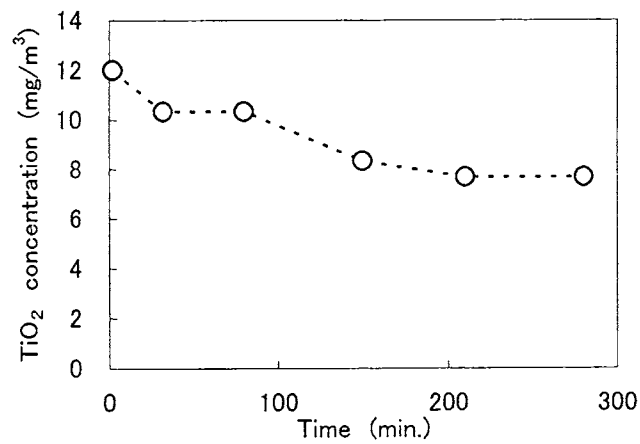

Fig.5 Change of TiO_2 concentration with time (T_1=75℃, T_2=1050℃)

Table 1 Experimental conditions

	Run 1	Run 2	Run 3	Run 4	Run 5
Total flow rate (*l*/min)	1.0	1.0	1.0	1.0	1.0
Ar gas flow rate (*l*/min)	0.2	0.2	0.2	0.2	0.2
Air flow rate (*l*/min)	0.8	0.8	0.8	0.8	0.8
Temperature of furnace reactor, T_1 (℃)	1000	1050	1050	1050	1050
Temperature of TTIP, T_2 (℃)	70	75	70	65	40
Residence time inside furnace reactor (s)	0.106	0.11	0.11	0.11	0.11

濃縮し、紫外線照射で生成したOHラジカルと効果的に反応させることが可能となると考えられる。すなわち、本方法は従来提案されている有害物質の除去・分解方法で必要な触媒量よりはるかに少量で同等の効率を達成できる可能性がある点で期待できる。

3 大気中ガス状・粒子状PAHs成分の分解特性の検討

前章のFig.4に示したラバールノズルで形成される超音速流れの上流に生成したナノ光触媒エアロゾルを希釈して連続的に導入し（Fig.7参照）、超音速ノズル部にUV光源から光を照射することで、大気エアロゾル中のガス状・粒子状PAHs成分を連続分解する試験を現在実施中であり、分析終了後に成果の公表を予定している。また、ガス状成分のみへの効果を確認するために、大気中PMをフィルターで捕集した後のガス成分への適用も予定している。

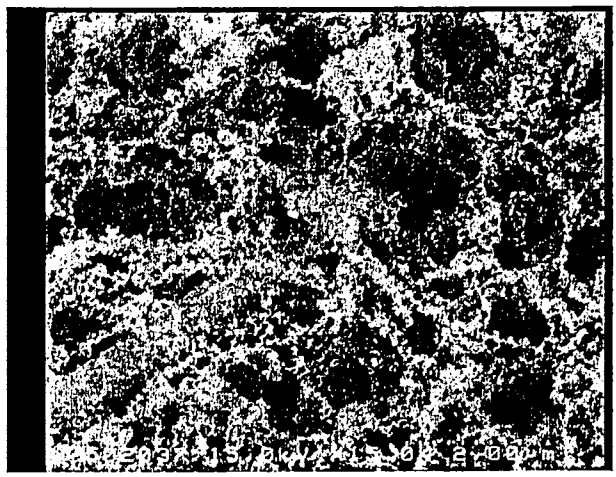

Fig.6 SEM photographs of collected TiO_2 particles on HEPA filter (Sampling time=30min, T_1=75℃, T_2=1050℃)

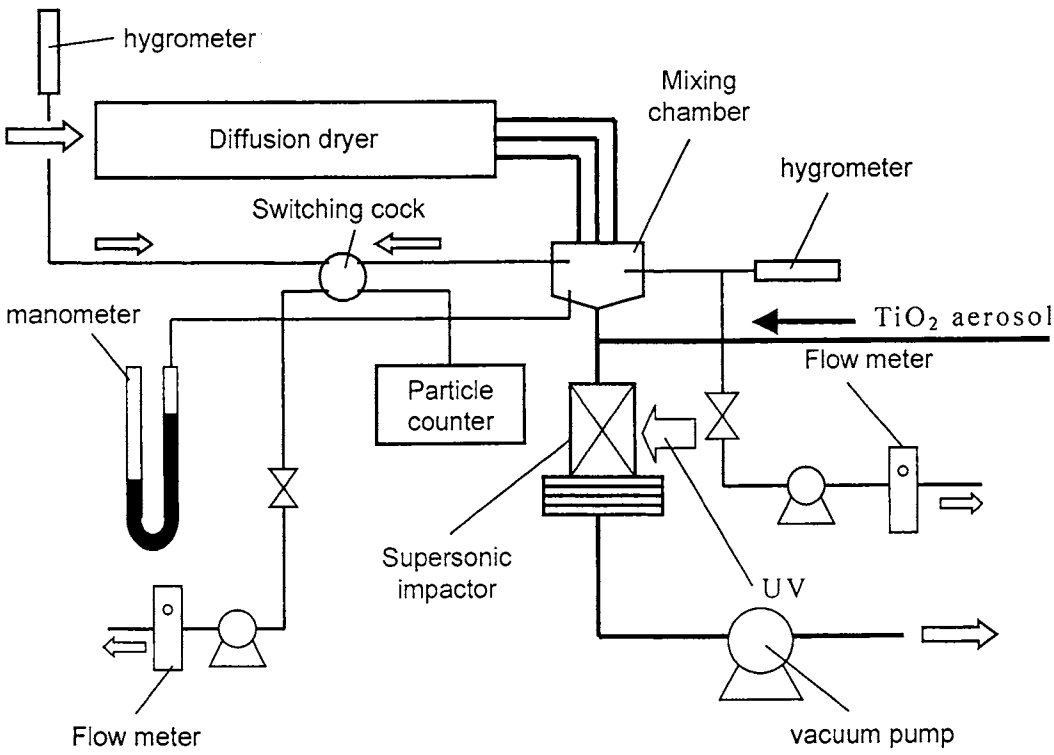

Fig.7 Experimental setup for ambient particle sampling

あとがき

本研究は平成１５年度～平成１６年度の間に、平成１５年度科学研究費（基盤研究（C）(2)）で実施した

「超音速流れ場中の液滴凝縮を利用したナノ大気エアロゾルとガス成分の同時測定」

の成果をまとめたものである。本研究の成果に基づいて、個々の検討項目により詳細な検討を加えるとともに、実用化・商品化を目指して行く予定である。